Protein Science (1996), 5:1026–1031. Cambridge University Press. Printed in the USA.

Mobile unnatural amino acid side chains in the core of staphylococcal nuclease

RICHARD WYNN,[1] PAUL C. HARKINS,[1,2,3] FREDERIC M. RICHARDS,[1] AND ROBERT O. FOX[1,2,4]

[1] Department of Molecular Biophysics and Biochemistry, Yale University, New Haven, Connecticut 06511
[2] Howard Hughes Medical Institute, Yale University, New Haven, Connecticut 06511

(RECEIVED March 6, 1996; ACCEPTED March 29, 1996)

Abstract

The structures of several variants of staphylococcal nuclease with long flexible unnatural amino acid side chains in the hydrophobic core have been determined by X-ray crystallography. The unnatural amino acids are disulfide moieties between the lone cysteine residue in V23C nuclease and methane, ethane, 1-*n*-propane, 1-*n*-butane, 1-*n*-pentane, and 2-hydroxyethyl thiols. We have examined changes in the core packing of these mutants. Side chains as large as the 1-*n*-propyl cysteine disulfide can be incorporated without perturbation of the structure. This is due, in part, to cavities present in the wild-type protein. The longest side chains are not well defined, even though they remain buried within the protein interior. These results suggest that the enthalpy–entropy balance that governs the rigidity of protein interiors favors tight packing only weakly. Additionally, the tight packing observed normally in protein interiors may reflect, in part, the limited numbers of rotamers available to the natural amino acids.

Keywords: protein dynamics; protein folding; protein structure; unnatural amino acids

The cores of globular proteins are well packed with hydrophobic side chains adopting discreet conformations. The role of tight packing in determining the detailed structure of a protein and its thermodynamic stability has been investigated extensively and reviewed recently (Richards & Lim, 1994). Upon folding, the side chains are substantially restricted in the conformations they explore, leading to an entropic penalty (recently reviewed by Doig & Sternberg [1995]). Would longer fatty acid-like side chains with many more degrees of freedom display different behavior when incorporated into protein cores? We have previously introduced a combined mutagenesis/chemical modification method that allows for the incorporation of unnatural amino acid side chains into protein cores (Wynn & Richards, 1993). This method relies on the chemical modification of a single cysteine residue introduced into the protein by conventional mutagenesis methods. Side chains with dramatically different properties or continuously varying properties can be introduced and the resultant protein characterized.

Staphylococcal nuclease is a nonspecific endonuclease. It is a paradigm protein for physical chemical studies. The structure has been determined previously by X-ray crystallography with (Loll & Lattman, 1989) and without (Hynes & Fox, 1991) the inhibitor pdTp and Ca^{+2} bound. The structure is made up of a six-stranded antiparallel β-barrel and three α-helices (Fig. 1A and Kinemage 1). Position 23 lies in the third strand and its side chain is directed toward the center of the β-barrel. It is surrounded predominantly by hydrophobic residues (Fig. 1B). The effects of mutations at position 23 has been examined previously (Shortle et al., 1990; Wynn et al., 1995). We have introduced a series of cysteine-*n*-alkane disulfide side chains at position 23 of staphylococcal nuclease with methane, ethane, 1-*n*-propane, 1-*n*-butane, 1-*n*-pentane thiols, and 2-hydroxyethyl (β-mercaptoethanol) thiols. We will refer to each protein variant by the thiol that is disulfide bonded to cysteine 23. Thus, the methane thiol-cysteine disulfide variant will be referred to as the methyl protein. Nuclease V23C with an unmodified cysteine will be referred to as the cysteine variant or the unmodified protein. The strictly aliphatic side chains continuously increase in volume, hydrophobicity, and flexibility. Volume and hydrophobicity would be expected to increase approximately linearly with side chain length, but the number of possible conformations taken up by a side chain should

Reprint requests to Richard Wynn at his present address: Dupont Merck Pharmaceutical Company, Rt. 141 & Henry Clay Rd., Experimental Station, E336/241B, Wilmington, Delaware 19880-0361; e-mail: wynnr@a1.lldmpc.umc.dupont.com.

[3] Present address: Department of Biochemistry, University of Texas Southwestern Medical Center, Dallas, TX 75235-5090.

[4] Present address: University of Texas, Medical Branch at Galveston, Department of Human Biological Chemistry and Genetics, Galveston, Texas 77550-1055.

Abbreviations: BME, β-mercaptoethanol; MD, molecular dynamics; pdTp, 3′,5′ thymidine diphosphate; SA, simulated annealing.

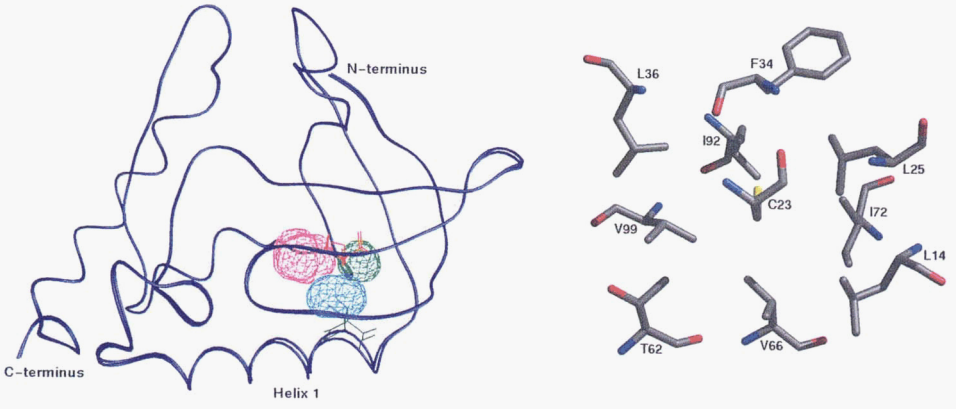

Fig. 1. A: Backbone trace of V23C-SH and V23C-SS-1-*n*-pentyl nuclease. Cavities are shown as mesh surfaces. Large and small cavities found in the unmodified protein are colored pink and green, respectively. The cavity found in the pentyl structure is colored cyan. Only the major conformation for Cys 23 for the unmodified protein was included for cavity detection. Cys 23 is shown in red. Val 66 is shown in green. This figure was produced using the Program GRASP (Nicholls et al., 1993). **B:** Residue 23 and surrounding amino acids. Atoms are colored according to atom type: carbon, gray; nitrogen, blue; oxygen, red; sulfur, yellow. Orientation from the backbone trace of Figure 1A is maintained.

increase geometrically with the number of rotatable bonds. The methyl cysteine disulfide side chain is approximately isosteric with methionine, the most flexible nonpolar natural amino acid. The pentyl derivative would have well over 1,000 potential rotamers. This would be expected to have a dramatic effect on the side-chain conformational entropy. Additionally, the propyl cysteine and 2-hydroxyethyl cysteine disulfide side chains are approximately isosteric with the terminal methyl group of the propyl chain being replaced by the potentially hydrogen bonding hydroxyl group. We have characterized the thermodynamic stability and the urea unfolded forms for these protein variants previously (Wynn et al., 1995). Here we report the high-resolution structures as determined by X-ray crystallography.

Results and discussion

Global structural change

There is little change in the global structures of these protein variants when compared with the structure for wild-type nuclease (Kinemage 2). As with the structure of wild-type staphylococcal nuclease-pdTp-Ca^{+2} complex, no electron density is observed for residues 1–6 and 142–149 (Loll & Lattman, 1989). The RMS deviation (RMSD) for all main-chain atoms between wild-type nuclease and the cysteine variant is 0.21 Å; the unmodified protein can therefore be considered a pseudo-wild type. The RMSD for all main-chain atoms varies from 0.13 Å (methyl-ethyl comparison) to 0.27 Å (methyl-butyl comparison) for the structures reported here. Analysis using difference distance matrices (Richards & Kundrot, 1988; program kindly provided by Dr. Patrick Fleming) for the methyl, ethyl, propyl, butyl, and BME structures using the unmodified cysteine variant as a reference structure shows changes greater than 0.5 Å only in the mobile loop regions of residues 46–49 and 115–118 in addition to the first and last residues observed in the electron density (residues 7 and 141, respectively). Analysis of the pentyl structure, however, shows large changes, often greater than 1 Å, in the region around residue 66, which lies at the carboxyl end of the first α-helix (see Fig. 1A). This helix packs into the β-barrel, positioning residue 66 near residue 23. Side chains as large as a butyl-cysteine disulfide do not perturb this region significantly. The pentyl-cysteine disulfide side chain is accommodated by a repositioning of helix 1 away from the β-barrel in a rigid body movement. Residues 54–66 keep main-chain dihedral angles and hydrogen bonding patterns characteristic of α-helices. The ϕ, ψ angles of residue 23 are not significantly different in any of these structures. The β-barrel region has been identified as an early folding intermediate by hydrogen exchange measurements (Jacobs & Fox, 1994). It is interesting to note that this region remains largely unperturbed when over-packed and helix 1, which has low amide protection factors in the folding intermediate, begins to move away.

Packing of interior residues

Analysis of the unmodified protein structure for cavities using the program GRASP (Nicholls et al., 1993) and a probe radius of 1.4 Å shows cavities of 59 $Å^3$ and 18 $Å^3$ adjacent to residue 23 in the cysteine variant (Fig. 1A). Cavities of the volumes observed here are unusual, but are observed occasionally in protein structures (Hubbard et al., 1994). The larger cavity is proximal to residue 23 and is surrounded by the side chains of residues Asp 21, Cys 23, Leu 36, Thr 62, Val 66, and Val 99. The smaller cavity is bounded by residues Cys 23, Leu 25, Val 66, Ile 72, and Ile 92. Similar cavities are found in the structure of the wild type nuclease-pdTp-Ca^{+2} complex (31 $Å^3$ and 17 $Å^3$).

The unmodified cysteine side chain clearly exists in two conformations (Fig. 2). Occupancy refinement suggests that the major conformer is populated 77% of the time, whereas the minor conformer is populated 22%. Multiple conformations within a protein interior are very rarely observed. In adopting both conformations, the cysteine residue approximates the size and shape of the wild-type valine side chain. The surrounding residues (Leu 25, Leu 36, Thr 62, Val 66, and Ile 92) undergo no side-chain rotations; the packing geometry in the wild-type structure is closely maintained. MD calculations do not show transitions between the two conformations during 50 ps of simulation. Close contacts of the Cys 23 side chain with the Cδ1 of Ile 92 (major conformation) and the Cγ2 of Thr 62 (minor con-

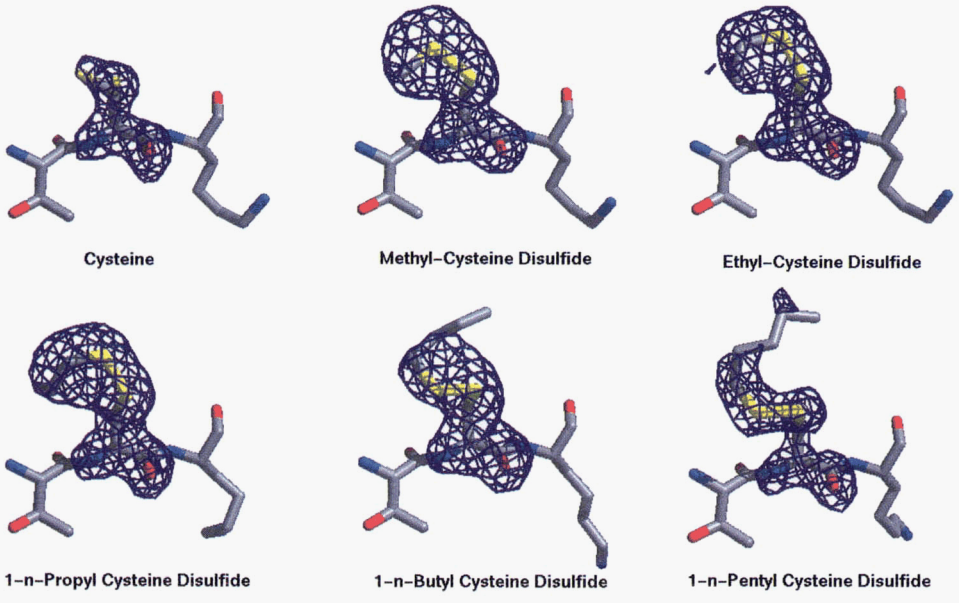

Fig. 2. $(F_o - F_c)$ position 23 omit maps contoured at 3.5σ. Maps were calculated in XPLOR (Brünger, 1992) and displayed using the program MIDAS (Computer Graphics Laboratory, University of California, San Francisco). Two rotamers for cysteine are shown in the stick model.

formation) presumably slow this rotation such that it is not sampled during our MD calculation.

The larger cavity in the unmodified protein is large enough to contain the additional size in the methyl-cysteine and ethyl-cysteine disulfide side chains (assuming atom volumes of Richards, 1977). In the methyl and ethyl proteins, only smaller cavities remain in either structure (19 Å^3 and 17 Å^3, respectively), and the methyl and ethyl side chains in fact pack into the large cavity adjacent to residue 23 and no change of the surrounding residues (Leu 25, Leu 36, Thr 62, Val 66, and Ile 92) is observed. Eriksson et al. (1992) have shown that cavity creation is destabilizing to protein structure and correlates well with thermodynamic stability for a series of mutants that replace buried large hydrophobic side chains with smaller ones. The increased stability (1.8 and 1.4 kcal/mol, respectively [Wynn et al., 1995]) observed for the methyl and ethyl mutants relative to the unmodified protein must be due, in part, to the elimination of cavity volume. However, we do not observe a correlation with thermodynamic stability as in the Eriksson et al. study. All side chains larger than the ethyl group represent overpacking of the protein core and structural responses to the mutation. In addition, we have observed large changes in the non-native forms of these proteins. Both native state structural perturbation and non-native state change would be expected to remove any simple correlation between thermodynamic stability and cavity volume.

The propyl protein has no detectable cavities using the 1.4-Å probe radius, although the structure remains apparently unchanged. The propyl side chain also projects into the large cavity, but close contacts between the propyl side chain and residues Gly 20, Leu 36, Thr 62, and Ile 92 force the sulfur atom of the propyl mercaptan group to fill the space that makes up the smaller cavity in the unmodified protein. Close contact of the carbon adjacent to sulfur in the propyl chain (C1) with Cδ of Ile 92 causes a rotation of Cδ of Ile 92 away from position 23. The positions of residues Leu 25, Leu 36, Thr 62, and Val 66 remain unchanged. Thus, the propyl side chain approaches the limit of volume that can be accommodated at position 23 without significant rearrangement. The BME structure is very similar to the propyl structure with the exception that Ile 92 does not undergo a change in rotameric form. As with the propyl structure, no cavities are detected. This again suggests that the propyl and BME groups approach the volume limit at position 23 in the nuclease structure. The hydroxyl group of the BME moiety forms a hydrogen bond to the carbonyl oxygen of residue 19. This additional specific interaction holds the terminal hydroxyl group in place (see discussion below).

These smaller side chains take up similar conformations with side-chain dihedral angles maintained. Respectively, for methyl, ethyl, propyl, and BME variants $\chi_1 = 65°, 59°, 68°, 59°$; $\chi_2 = -130°, -156°, -151°, -157°$; $\chi_3 = 82°, 87°, 96°, 92°$. Note that the χ_3 values, which correspond to the disulfide dihedral angle, lie close to the minimum at 90°. In the butyl and pentyl variants, the large side chains can no longer be accommodated in the cavities existing in the unmodified protein. This is reflected by a shift in the side-chain dihedrals: for butyl and pentyl structures, respectively, χ_1 is 69° and 57°; χ_2 is −85° and −82°; χ_3 is −79° and −69°. Notably, the disulfide torsional angle switches to near the opposite minimum (−90°) to that observed (+90°) for the variants with smaller side chains. The side chains of Leu 14, Leu 25, Phe 34, Leu 36, Thr 62, Val 66, Ile 72, and Val 99 all contact these larger side chains, but maintain rotameric form. The main adjustment to these larger side chains, particularly noticeable in the pentyl variant, is the displacement of helix 1 from the main body of the β-barrel. The result of this movement is that the butyl and pentyl variants each show a single cavity (17 Å^3 and 29 Å^3, respectively). Thus, even with these very flexible side chains, space cannot be completely filled; packing defects do occur. The cavity in the pentyl mutant lies below

strand 2 and just above strand 1 and helix 1 (Fig. 1A). It is surrounded by residues Leu 14, Ala 17, Cys-Pen 23, Thr 62, and Val 66.

Protein dynamics

($F_o - F_c$) maps of these side chains displayed at 3.5σ (Fig. 2) show that the observed electron density does not cover the entire hydrocarbon moiety for the propyl, butyl, and pentyl variants. *B*-factors for the pentyl group atoms range from 40 to 50 Å^2, for the propyl group range from 40 to 55 Å^2, whereas for the butyl group, they range from 70 to 90 Å^2. Omit maps at lower contour levels delineate the entire pentyl and propyl side chains, whereas density for the three terminal carbons of the butyl moiety does not appear before the noise. The surrounding residues are well defined by the observed electron density and the *B*-factors for these residues are not significantly higher than those of the unmodified protein structure. These data indicate that the terminal atoms in the longer alkanethiol cysteine disulfide side chains are undergoing increased motion relative to the surrounding residues or that these side chains are populating multiple conformations. The higher *B*-factors and lack of density at lower contour levels for the butyl group relative to the pentyl and propyl groups suggests that this effect is more pronounced in the butyl case.

Ten SA refinements, followed by rounds of positional and restrained *B*-factor refinement, did not yield significantly different conformations for the butyl side chain. Although 12 similar refinements of the pentyl structure did result in two structures with different conformers for the pentyl side chain, these two had significantly higher calculated energies than the conformation shown in Figure 2. Fifty-picosecond MD trajectories for the butyl variant give higher RMS displacements for the butyl group than for any of the surrounding side chains (Fig. 3). The Cδ atoms of Ile 72 and Ile 92 also show high mobility due to a tendency for rotamer flips about χ_2. A similar MD simulation for the pentyl variant does not yield significantly higher RMSD values for the pentyl group relative to the surrounding side chains. This probably reflects less motion for the pentyl group than for the butyl, as indicated by the electron density and *B*-factor patterns discussed above. The MD calculations suggest that the dynamic behavior observed here could be the result of motion around a single conformation. The lack of alternate conformations found during multiple SA refinements also supports this hypothesis, although we cannot rigorously rule out alternate side-chain conformations not sampled during our calculations.

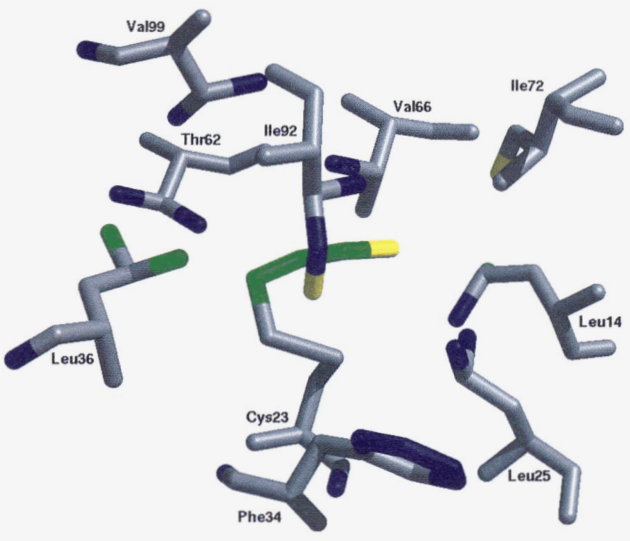

Fig. 3. Side-chain packing around the butyl moiety. Atoms were color coded according to the RMSD from the average structure during a 50-ps MD trajectory. Gray, RMSD less than 0.3 Å; blue, RMSD between 0.3 Å and 0.4 Å; green, RMSD between 0.4 Å and 0.5 Å; yellow, RMSD greater than 0.5 Å.

Assuming a relatively rigid backbone scaffold, small amplitude bond vibrations and torsional angle oscillations could add up throughout these very long side chains, producing the behavior observed here. The resultant motions would increase with each additional side-chain bond; atoms further from the main chain would display larger amplitude motions and consequently electron density would be more difficult to measure and the *B*-factors would increase. This behavior is analogous to the motions of long chain fatty acids embedded in lipid bilayers, where order parameters decrease for carbons atoms further away from the lipid head group. Amplified motion of this type is unlikely to occur with the normal amino acids because the number of freely rotatable bonds is limited to three for the nonpolar naturally occurring amino acids (methionine). Comparison of the propyl and BME structures supports this hypothesis. As discussed above, the hydroxyl group of the BME group forms a hydrogen bond to the carbonyl of residue 19 (see Fig. 4). This limits the motion of the BME group, thereby decreasing the number of freely rotating bonds from an "anchor" point. The corresponding omit maps are displayed in Figure 4. Full electron density is observed for the BME moiety, reflecting decreased motion for this group. The *B*-factors for the BME moiety are also considerably lower than those of the propyl moiety (30–40 Å^2 as compared with 40–55 Å^2).

Protein folding is opposed by side-chain configurational entropy (Doig & Sternberg, 1995; Bromberg & Dill, 1994). The configurational entropy can be divided into two terms, conformational entropy and vibrational entropy. The conformational entropy loss is associated with a decrease in the number of rotamers sampled by the native state relative to the unfolded form. The vibrational entropy loss is related to the potential damping of vibrational and oscillational motions in a given rotamer by the tight packing in a protein interior. Creamer and Rose (1992) have also suggested that side-chain entropy can account for the different helix-forming propensities of natural amino acids. The large number of high-resolution protein structures clearly show that conformational entropy loss does occur upon folding; side chains populate only a single rotamer in the native state. We have tentatively concluded, on the basis of MD and SA calculations, that this conformational entropy loss also occurs with the long flexible amino acid side chains studied here. However, the dynamics observed for these side chains suggest that vibrational entropy loss is not severe, a result suggested previously from MD simulations (Karplus et al., 1987). The apparent motion observed here suggests that the entropy–enthalpy balance that governs the rigidity of protein interiors only weakly favors tight packing—the addition of only a few extra bonds results in greatly increased thermal motion. This result is reminiscent of the ability of many proteins to form molten globule states. A corollary to these results would be that the tight packing ob-

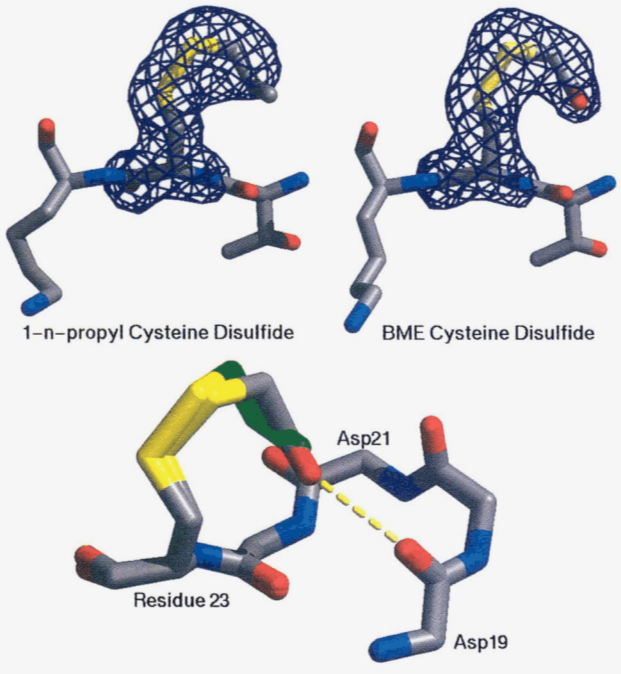

Fig. 4. Comparison between propyl and BME variant structures. Top: Position 23 omit maps. Right, propyl variant; left, BME variant. See Figure 2 legend for details. Bottom: Superimposition of the propyl and BME variant structures. Atom colors denote atom type except for the propyl hydrocarbon chain, which is shown in green. The hydrogen bond between the BME hydroxyl group and the main-chain carbonyl oxygen of Asp 19 is shown by the dotted line.

served in protein interiors is due, in part, to the limited number of rotamers available to the natural amino acids.

Finally, the introduction of unnatural amino acids into the core of staphylococcal nuclease has allowed us to follow the response of the protein structure as the side chain at position 23 is made larger by increments of a single methylene group. A similar series at a single position is not possible using conventional mutagenesis procedures. Additionally, these very long flexible side chains apparently undergo considerable thermal motion relative to "normal" buried amino acid side chains—a behavior not likely to be observed with natural amino acids. Thus, side chains with very different physical properties may provide an approach for determining the balance of the many forces that drive folding and binding processes.

Materials and methods

The nuclease mutants used in this study were produced as described by Wynn et al. (1995). Proteins complexed to pdTp and Ca^{+2} were crystallized as described previously (Loll & Lattman, 1989). Diffraction data were collected from single crystals of each variant at 5.0 °C using a MacScience Dip-2000 IP system. The X-ray data statistics are presented in Table 1.

The starting phases and coordinates for all structures were derived from the structure of the nuclease A-pdTp-Ca^{+2} complex (Loll & Lattman, 1989). Residue 23 was omitted from early refinement procedures. Rigid body refinement was conducted using the low-resolution diffraction data (15–3 Å). An overall anisotropic temperature factor was then computed and applied to the model. Several rounds of positional and individual restrained *B*-factor refinement (Brünger, 1992) were performed. The SA omit procedure (Hodel et al., 1992) was conducted, followed by introduction of waters into peaks of the $F_o - F_c$ maps at contours no lower than 3σ using XPEAKS and GETUNIK (J. Wang). Waters that had post-refinement temperature factors greater than 60.0 were removed from the structures followed by positional and *B*-factor refinement. All refinement procedures were conducted in the program X-PLOR (Brünger, 1992). Electron density maps were calculated and visualized using the program XtalView (McRee, 1992).

MD calculations were performed starting from the refined coordinates using X-PLOR (Brünger, 1992). Symmetry-related electrostatic and Van der Waals energy terms were included in the potential function. A 1-fs step size time step was used. Ini-

Table 1. *X-ray data statistics*

	PSH	Methyl	Ethyl	Propyl	Butyl	Pentyl	BME
Space group	$P4_1$	$P4_1$	$P4_1$	$P4_1$	$P4_1$	$P4_1$	$P4_1$
$a = b$ (Å)	47.4	48.6	48.5	48.3	48.5	47.8	48.2
c (Å)	62.8	63.4	63.2	63.1	63.1	62.6	63.0
Resolution range (Å)	6.0–1.90	6.0–2.10	6.0–2.00	6.0–1.90	6.0–2.00	6.0–2.10	6.0–1.96
No. of unique reflections	9,359	7,358	9,282	10,289	8,454	6,914	9,191
% Unique reflections	87.9	88.7	89.0	92.8	91.1	87.4	91.6
High resolution bin	1.98–1.90	2.19–2.10	2.08–2.00	1.98–1.90	2.09–2.00	2.19–2.10	2.05–1.96
% Complete	76.5	81.5	77.0	82.2	75.4	85.6	75.8
R-factor[a]	0.173	0.181	0.179	0.171	0.174	0.169	0.169
R-merge[b]	0.069	0.051	0.054	0.049	0.059	0.060	0.058
Redundancy	3.7	5.6	5.8	5.2	5.7	6.3	4.1
No. of water molecules	39	32	35	51	42	38	45
Mean *B*-factor:							
Main-chain atoms	33.2	36.7	35.4	32.2	37.6	28.9	35.7
Side-chain atoms	37.4	41.2	39.6	36.4	41.8	32.5	39.6

[a] $R\text{-factor} = \sum_{h,k,l} \left| |F_{obs}(h)| - k|F_c(h)| \right| / \sum_{h,k,l} |F_{obs}(h)|$.
[b] $R\text{-merge} = \sum (\text{Abs}(I - \langle I \rangle)) / \sum \langle I \rangle$.

tial velocities were assigned to a Maxwellian distribution and the method of Berendsen (1984) was used for temperature coupling (277 K). Slow-cooling SA calculations after the method of Brünger et al. (1990) using a variety of initial temperatures (between 1,500 and 2,500 K) and a cooling step size of 25 K were used to search for potential alternate conformations. Slow-cooling SA calculations were followed by one round each of positional and individual restrained *B*-factor refinement as described above.

Acknowledgments

We thank the following for helpful discussions and technical assistance: Patrick Fleming, Alan Friedman, Marc Jacobs, Wendell Lim, Jimin Wang, Joseph Yaeger, Luke Rice, and Sarina Bromberg.

References

Berendsen HJC, Postma JPM, van Gunsteren NF, DiNola A, Haak JR, 1984. Molecular dynamics with coupling to an external bath. *J Chem Phys 81*:3684–3690.

Bromberg S, Dill KA, 1994. Side-chain entropy and packing in proteins. *Protein Science 3*:997–1009.

Brünger AT. 1992. *X-PLOR manual, version 3.0*. New Haven, Connecticut: Yale University.

Brünger AT, Krukowski A, Erickson J. 1990. Slow-cooling protocols for crystallographic refinement by simulated annealing. *Acta Crystallogr A 46*:585–593.

Creamer TP, Rose GD. 1992. Side-chain entropy opposes helix formation but rationalizes experimentally determined helix-forming propensities. *Proc Natl Acad Sci USA 89*:5937–5941.

Doig AJ, Sternberg MJE. 1995. Side-chain conformational entropy in protein folding. *Protein Sci 4*:2247–2251.

Eriksson AE, Baase WA, Zhang XJ, Heinz DW, Blaber M, Baldwin EP, Matthews BW. 1992. Response of a protein structure to cavity-creating mutations. *Science 255*:178–183.

Hodel A, Kim SH, Brünger AT. 1992. Model bias in macromolecular crystal structures. *Acta Crystallogr A 48*:851–858.

Hubbard SJ, Gross KH, Argos P. 1994. Intramolecular cavities in globular proteins. *Protein Eng 7*:613–626.

Hynes TR, Fox RO. 1991. The crystal structure of staphylococcal nuclease refined at 1.9 Å. *Proteins Struct Funct Genet 10*:92–105.

Jacobs MD, Fox RO. 1994. Staphylococcal nuclease folding intermediate characterized by hydrogen exchange and NMR spectroscopy. *Proc Natl Acad Sci USA 91*:449–453.

Karplus M, Ichiye T, Pettit BM. 1987. Configurational entropy of native proteins. *Biophys J 52*:1083–1085.

Loll PJ, Lattman EE. 1989. The crystal structure of the ternary complex of staphylococcal nuclease, Ca^{+2}, and the inhibitor pDTp, refined at 1.65 Å. *Proteins Struct Funct Genet 5*:183–201.

McRee DE. 1992. A visual protein crystallographic software system for X11/XView. *J Mol Graphics 10*:44–46.

Nicholls A, Bharadwaj R, Honig B. 1993. GRASP graphical representation and analysis of surface properties. *Biophys J 64*(Part 2):A166.

Richards FM. 1977. Areas, volumes, packing and protein structures. *Annu Rev Biophys Bioeng 6*:151–176.

Richards FM, Kundrot CE. 1988. Identification of structural motifs from protein coordinate data secondary structure and first-level supersecondary structure. *Proteins Struct Funct Genet 3*:71–84.

Richards FM, Lim WA. 1994. An analysis of packing in the protein folding problem. *Annu Rev Biophys Bioeng 26*:423–498.

Shortle D, Stites WE, Meeker AK. 1990. Contribution of the large hydrophobic amino acids to the stability of staphylococcal nuclease. *Biochemistry 29*:8033–8041.

Wynn R, Anderson CL, Richards FM, Fox RO. 1995. Interactions in nonnative and truncated forms of staphylococcal nuclease as indicated by mutational free energy changes. *Protein Sci 4*:1815–1823.

Wynn R, Richards FM. 1993. Unnatural amino acid packing mutants of *Escherichia coli* thioredoxin produced by combined mutagenesis/chemical modification techniques. *Protein Sci 2*:395–403.